machines

MDPI

Article

Synthesis of Mechanisms Based on Optimal Solution Density

Sean Mather and Arthur Erdman *

Mechanical Engineering Department, University of Minnesota, 111 Church St. S.E., Minneapolis, MN 55455, USA; mathe587@umn.edu

* Correspondence: agerdman@umn.edu

Abstract

The traditional process for kinematic synthesis of planar mechanisms involves setting a few prescribed positions, then solving a set of equations to identify a vector chain that exactly reproduces those positions. In evaluating these equations, designers often must sift through multiple "infinities" of solutions corresponding to some number of free-choice variables that each have an infinite number of possible values. In this vast solution space, some combination of those variables will produce the most optimal solution, but finding that optimal solution is not trivial. There are two extremes for addressing the impossibility of sifting through infinite possible values. First, one could use analytical techniques to make educated estimates of the optimal values. Or, alternatively, a designer could completely remove their perspective from the process, passing the problem into a computer and programming it to sift through millions (or orders of magnitude more) possible solutions. The present work proposes a novel intermediate step in the analytical synthesis process that functions as a middle ground between these extremes. Optimizing solution density involves a designer manually manipulating the problem definition to increase the percentage of solutions that have pivots in acceptable locations. This is accomplished by changing the values of δ_j and α_j (prescribed translation and rotation of the moving plane, respectively) to manipulate the position of the poles. A physical example, designing a 7-bar parallel-motion generator, shows that applying this method yields more passing solutions when comparing over the same search depth. Specifically, 0.008% of solutions pass the design criteria without applying the method, and 3.154% pass after optimizing. This approach can reduce the computational load placed on a computer running a search script, as designers can use larger increments on the free choices without skipping over a family of solutions.

Keywords: solution density; kinematic synthesis; MK circle; planar mechanisms

check for updates

Academic Editor: Dan Zhang

Received: 29 July 2025
Revised: 20 August 2025
Accepted: 25 August 2025
Published: 28 August 2025

Citation: Mather, S.; Erdman, A. Synthesis of Mechanisms Based on Optimal Solution Density. *Machines* **2025**, *13*, 773. https://doi.org/10.3390/machines13090773

Copyright: © 2025 by the authors. Licensee MDPI, Basel, Switzerland. This article is an open access article distributed under the terms and conditions of the Creative Commons Attribution (CC BY) license (https://creativecommons.org/licenses/by/4.0/).

1. Introduction

Linkage mechanisms are often underappreciated, but they are one of the key drivers of motion in the world. Examples are found in everything from engines to cranes, as well as in hinges, exercise equipment, and surgical tools. Their modern ubiquity owes largely to the long history of study of kinematic synthesis, with some of the foundational work dating back to the mid-19th century, though no generalized analytical solution procedure was developed at this time [1,2]. In the mid-20th century, researchers like Freudenstein and Sandor resumed the work and identified many of the key principles of modern kinematic synthesis methods [3–6]. During these early years, a technique emerged that is still in use today, involving the division of a mechanism's topology into dependent kinematic chains. These chains are commonly known as dyads, triads, etc., according to their number of links. An example is shown in Figure A1.

Many authors have furthered this method of dividing a topology into vector loops. It is the principal method demonstrated in Sandor and Erdman's Advanced Mechanism Design texts [7,8]. Commonly, these kinematic chains are set to accomplish a path, motion, or function generation task. Of these, the motion generation task is the most restrictive, requiring that a point on the mechanism pass through a series of positions and that a link on the mechanism rotate through a corresponding set of angles. Each pair of a positional and angular displacement (δ, α) is referred to as a prescribed position. Researchers like Chase, Riley, and Erdman, or Lin, showed the method could be applied to triad chains [9,10]. Others found how many positions could be prescribed while preserving an exact solution to the problem [11,12]. For dyads, a designer can specify anywhere between two and five of these prescribed positions and still identify an exact solution. Diab used dyads to synthesize four-bar motion generators that also included prescribed velocities or accelerations [13]. Similar vector-based methods that do not use complex numbers have also found success, like those demonstrated by Midha and Zhao [14].

Traditionally, the designer specifies their set of prescribed positions, then manipulates free-choice variables to find an exact solution to the problem. While generally effective, the requirement that the solution exactly reach each prescribed position is often unnecessarily restrictive, limiting the solution space. Consider, for example, a pick-and-place operation. The linkage will drop down to an exact position to pick up a part, then translate over to a final exact drop-off position to release the part. The first and last positions need to be precise, but oftentimes, what the mechanism does in between these positions matters very little. Perhaps the mechanism needs to remain relatively close to a vertical orientation to avoid spilling any contents, and it may need to approach the final position from above to avoid striking an obstacle on the ground. Even with these interstitial requirements, though, the exact intermediate position often remains unnecessary; a designer may benefit the most from the ability to specify an approximate region as a prescribed position, allowing some extra space to mitigate the consequences of their uncertainty on the solution space. This realization gave rise to the optimal approximate and mixed exact-approximate prescribed position synthesis approaches [15–20]. Other authors have also expanded this idea to include optimization techniques [21,22]. In this framework, the designer specifies some (or sometimes, zero) exact positions, then adds a finite number of approximate positions. Replacing exact prescribed positions with approximate ones expands the solution space and increases the probability of finding a solution with favorable properties like high mechanical advantage or transmission angles, but also makes the problem more complex. Liu et. al. combined exact positions with approximate ones, and used a numerical atlas technique to obtain an initial estimate for link dimensions, in theory simplifying the overall calculation [23].

Other researchers have gone beyond mixing exact and approximate synthesis to pursue optimal approximate numerical methods, a trend that has increased correspondingly as computer capabilities have improved. Genetic algorithms, which find optimal solutions by emulating the ideas of natural selection, are one of the most common approaches within numerical methods [24–29]. Other approaches have included least squares or homotopy [30–33], neural networks [34,35], state-space models [36], and multiobjective synthesis [37,38]. Kim et. al., for example, applied machine learning to the synthesis of four-bar function generators in exact or approximate prescribed positions. Their approach uses a mixture of experts' frameworks to identify optimal solutions across many four-bar variants (crank-rocker, rocker-rocker, etc.) [39]. Zhang et. al. used genetic algorithms to generate 1-DOF six-bar mechanisms capable of replicating multiple target curves through an adjustable input parameter [40].

One computational approach that still finds exact solutions is commonly known as a 'grid search,' or sometimes a global search. While no computer can search through the infinite number of possible combinations of the free-choice variables, a script could feasibly search through a few million or even billions of possible combinations given enough time. This type of wide-ranging search increases the chances of finding a good solution, but is also computationally expensive and time-consuming, as an uninformed search must sift through huge quantities of bad options on the way to the final solution. The proposed technique in this manuscript will be compared against this blind grid-search approach as a benchmark for its effectiveness.

Much of the work in the exact synthesis analytical area has been building on the framework of loop-based kinematic synthesis, developing new methods that make more complex problems possible to solve or new tools for designers to visualize problems. For example, Lin and others' work on the compatibility linkage, a method for solving nonlinear systems of equations arising in kinematics [10,41–43]. Others have applied Freudenstein's method for analytical synthesis to geared linkages [44,45]. A visualization tool based on loop-based synthesis was uncovered by Loerch, called the MK Circles [46,47]. Loerch discovered that if one of the free-choice variables is held constant while the other is iterated from 0° to 360° (commonly β_2 and β_3), the solutions for both the ground and moving pivots settle into circles as shown in Figure 1. By itself, this finding is already a valuable synthesis and visualization tool for analyzing the mechanism solution space. One other item to note from Figure 1 is the dispersion of the potential pivot points. The figure was generated using a constant value of β_2 and varying β_3 by a uniform increment of 1° (the opposite case with constant β_3 is shown in the Appendix A in Figure A3). The resulting solutions, though, are not evenly dispersed in the plane. Instead, there is a high concentration of both moving pivot and ground pivot solutions centered about the pole P_{13}. This is the concept referred to in this paper as "solution density." The density, in terms of pivot points per unit of planar area, decreases further away from the poles.

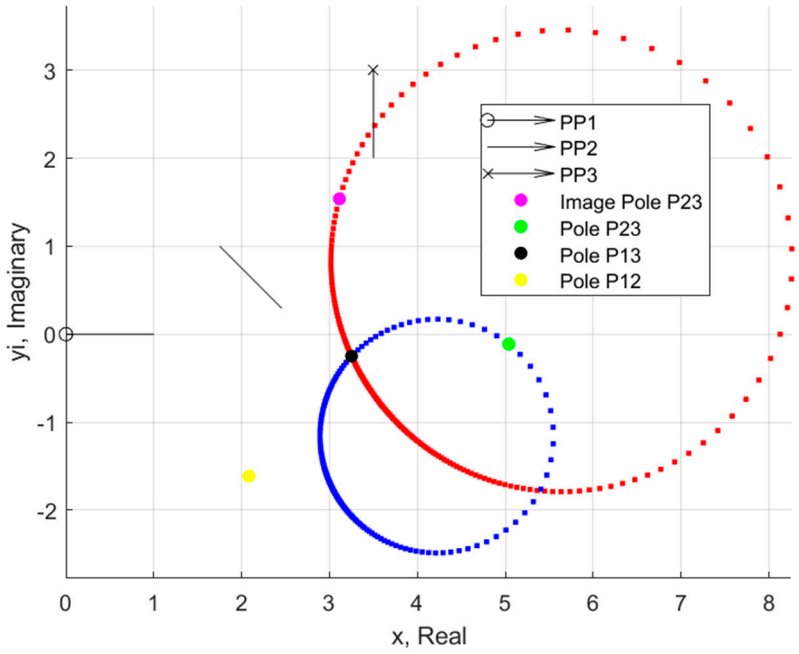


Figure 1. The MK Circles for a dyad in three positions. The blue points represent ground pivot locations, while red points represent moving pivots. $\boldsymbol{\delta_2}$ = 1.75 + 1i, $\boldsymbol{\delta_3}$ = 3.5 + 3i, $\alpha_2 = -45°$, $\alpha_3 = -90°$, $\beta_2 = -85°$.

The MK Circles have a clear relationship with the poles, as each circle will pass through at least two poles. The poles have significance outside of the circles, though. Each pole represents a geometric special case of the kinematic synthesis problem. For example, if the free choice β_2 is equal to α_2, that means that the first and second links of the dyad chain are rotating by the same amount between positions one and two. The practical effect is that the link behaves like a rigid line between the ground pivot and the prescribed position. There is only a single position in the plane about which a straight line can rotate to replicate the pose and angle of two unique prescribed positions [8]. The other pole locations have similar geometric explanations, which are summarized in Table 1, along with equations for finding their locations. The general forms are given in Reference [48]. Adding a fourth position adds three more poles—P_{14}, P24, and P_{34}—but also changes the behavior of solutions in the plane. When all four positions are considered, as the free-choice variable is iterated, the solutions settle into a cubic curve called the Burmester Curve that passes through a set of six of the poles and image poles. Mirth and Mlinar investigated how these curves change as a design parameter is varied, creating what Mlinar calls "the Burmester Field" [48–50].

Table 1. Pole Locations and Special Case Conditions.

Chain Type	Pole	Special Case	Moving/Ground	Physical Explanation	Equation *
Dyad	P12	$\beta_2 = \alpha_2$	Ground	Between P1 and P2, **W** ** and **Z** rotate as though they are a single rigid link	$P_{12} = \frac{\delta_2}{1-e^{i\alpha_2}}$
Dyad	P13	$\beta_3 = \alpha_3$	Ground	Between P1 and P3, **W** and **Z** rotate as though they are a single rigid link	$P_{13} = \frac{\delta_3}{1-e^{i\alpha_3}}$
Dyad	P12	$\beta_2 = 0$	Moving	Between P1 and P2, **W** has not moved	$P_{12} = \frac{\delta_2}{1-e^{i\alpha_2}}$
Dyad	P13	$\beta_3 = 0$	Moving	Between P1 and P3, **W** has not moved	$P_{13} = \frac{\delta_3}{1-e^{i\alpha_3}}$
Dyad	P23	$\beta_3 - \beta_2 = \alpha_3 - \alpha_2$	Ground	Between P2 and P3, **W** and **Z** rotate as a single link	$P_{23} = \frac{\delta_3 e^{i\alpha_2} - \delta_2 e^{i\alpha_3}}{e^{i\alpha_2} - e^{i\alpha_3}}$
Dyad	P23′	$\beta_2 = \beta_3$, $\alpha_2 \neq \alpha_3$	Moving	P1 and P2 are reached from the same moving pivot location k_1	$P'_{23} = \frac{\delta_2 - \delta_3}{e^{i\alpha_3} - e^{i\alpha_2}}$

* Note that all equations output vectors showing pole positions relative to PP1. ** All bolded quantities are vectors, while non-bolded quantities are scalars

The effect of the poles is significant for finding ideal solutions, especially when ground or moving pivots must be in a prescribed region, but it also has implications for manufacturing tolerances and linkage performance. Similar properties were observed by Faik, who investigated mechanism design sensitivity. He defines sensitivity as "the ratio of the change of a given output variable to the change in a design parameter [51]." As a mechanism's sensitivity value increases, so too does the impact of manufacturing inaccuracies on the output of the mechanism. In essence, manufacturing tolerances must be tighter when sensitivity is high to ensure the mechanism performs as designed. Several other authors also investigated the effect of tolerances on mechanism performance, or applied a similar sensitivity lens in mechanism synthesis [37,52–54].

2. Principles of Solution Density

To demonstrate the principles of solution density, a generic numeric example is provided. In Figure 2a, 20 points are plotted, ranging from 10 degrees below to 10 degrees above the value of β_3 that yields the pole location P_{13}. The linear distance between the first and last ground pivot locations is 0.5487, and the linear distance between the first and last moving pivot locations is 0.3309. In Figure 2b, an identical 20° range of values of β_3 is shown, but this time the range is from a lower bound of 20° to an upper bound of 40°. These items and the prescribed positions are summarized in Table 2.

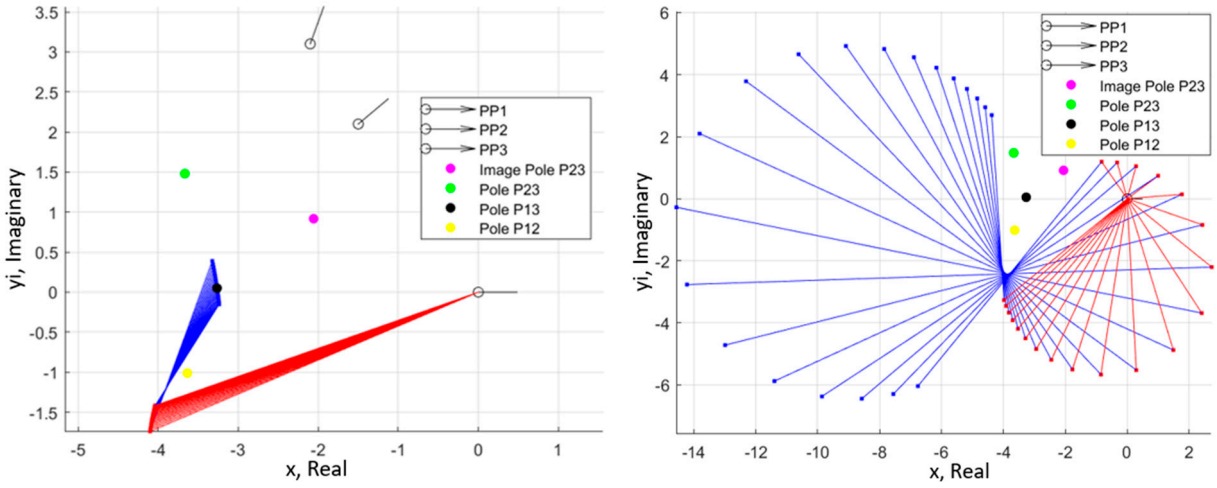


Figure 2. The results of plotting the problem situation described in Table 2. (**a**) The solutions are plotted for the β_3 range from 60–80°. (**b**) The solutions are plotted for the β_3 range from 20–40°.

Table 2. Example Problem Situation.

Position	δ	α	β
2	−1.5 + 2.1i	40°	15
3	−2.1 + 3.1i	70°	(a) 60–80° (b) 20–40°

Despite plotting an identical angle input range, the second case results in answers spanning nearly the entire circumference of both the M and K circles. In that case, the distance between the furthest points is just the diameter of each circle, or 11.381 and 6.863 units for the M and K circles, respectively. At the widest point, the distance between two consecutive points is 2.4934. That is greater than the entire 20° interval plotted near the pole location in (a). The pair of figures reveals how dramatic the effect of solution density is on the solution space. Given these findings, a key question that emerges is, 'How might a designer take advantage of the concept of solution density?' We propose using a mixed exact-approximate problem definition to invert the synthesis process. Rather than applying a method like ground pivot specification [8] to a set of prescribed positions, in this approach, the designer finds a solution in the desired ground pivot region by adjusting the prescribed information to manipulate the pole locations.

For example, in the case presented in Table 2, the region of greatest solution density is concentrated around −3 + 0i. Plotting the entire range of β_2 and β_3 reveals the plot shown in Figure 3. Both β_2 and β_3 are iterated in two-degree increments from 0 to 360 degrees. Recall from Figures 1 and A3 that all ground pivot circles pass through the pole P_{23}, regardless of which free-choice variable is held constant. If the angle β_2 is held constant and the value of β_3 is iterated from 0 to 360°, the ground pivot circle will also include the point pole P_{13}. Similarly, if the angle β_3 is held constant and the value of β_2 is iterated from 0 to 360°, the ground pivot circle will always include the point pole P_{12}. This is due to the special-case conditions shown in Table 1 that produce pole locations. The pole P_{12} is a ground pivot solution when $\beta_2 = \alpha_2$, a condition that will always be activated if all 360 degrees of the possible range of β_2 are considered. The same is true for pole P_{13} when $\beta_3 = \alpha_3$. Finally, P_{23} is a ground pivot solution that is found when $\beta_2 = \beta_3$, a condition that is reached regardless of which variable is iterated. The resulting pole triangle (P_{12}–P_{23}–P_{13}) is the confluence in the plane with the highest solution density.

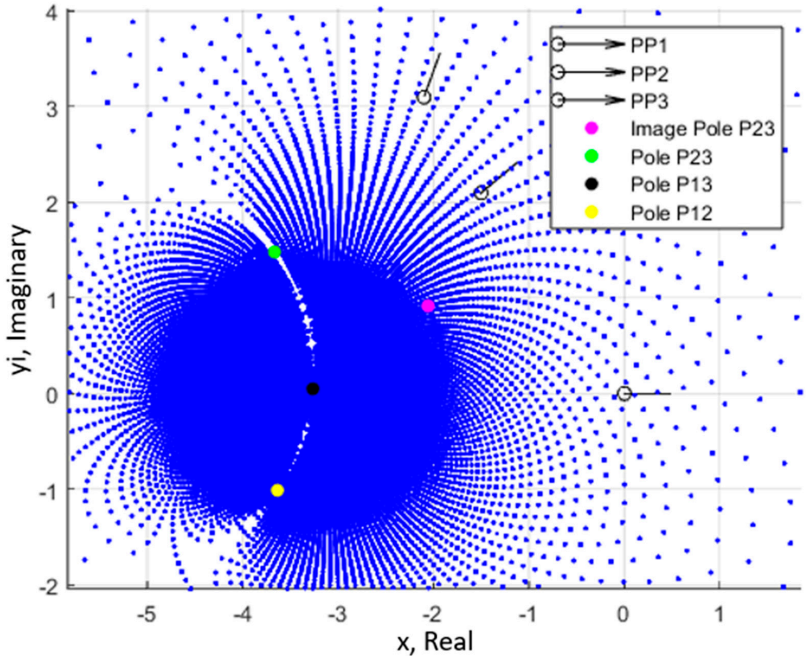


Figure 3. The M circles are plotted for the problem case shown in Table 2. Both β_2 and β_3 are iterated in two-degree increments from 0 to 360 degrees.

Suppose the mechanism designer hopes to perform a pick-and-place operation with an exact first and third position. In that case, they can still manipulate the location of the pole triangle by adjusting the position and orientation of the second prescribed position. A ground pivot location above and to the right of the prescribed positions (i.e., at 0 + 3i) may be desirable to avoid an obstacle in the workspace. The initial problem configuration centers the pole triangle (and consequently the region of greatest solution density) around (−3 + 0i). If position 2 is held in place, but the angle is increased by 180° to 220°, the poles P_{23} and P_{12} shift to a position above the prescribed points, as shown in Figure 4. Combining rotation with moving the second precision position can have an even greater effect, as shown in Figure 5.

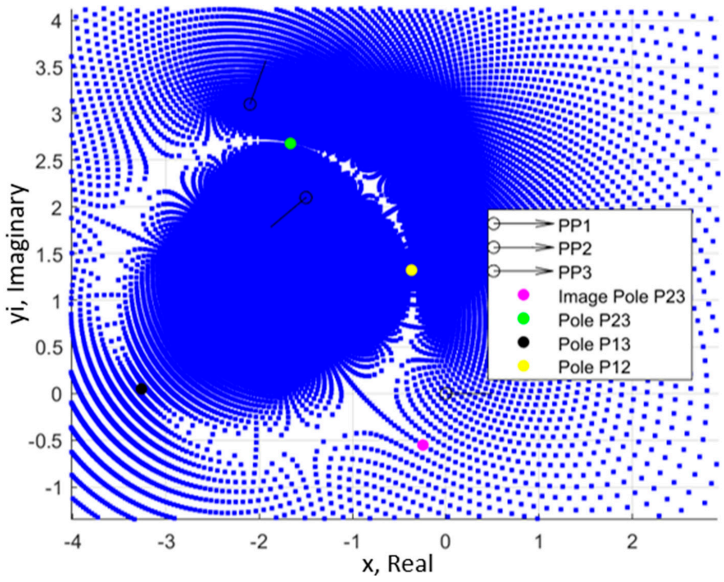


Figure 4. Shifting the locations of P_{23} and P_{12} by manipulating the angle α_2 at the second prescribed position. Note that positions PP1 and PP3 are unchanged, while the angle of PP2 is rotated 180°.

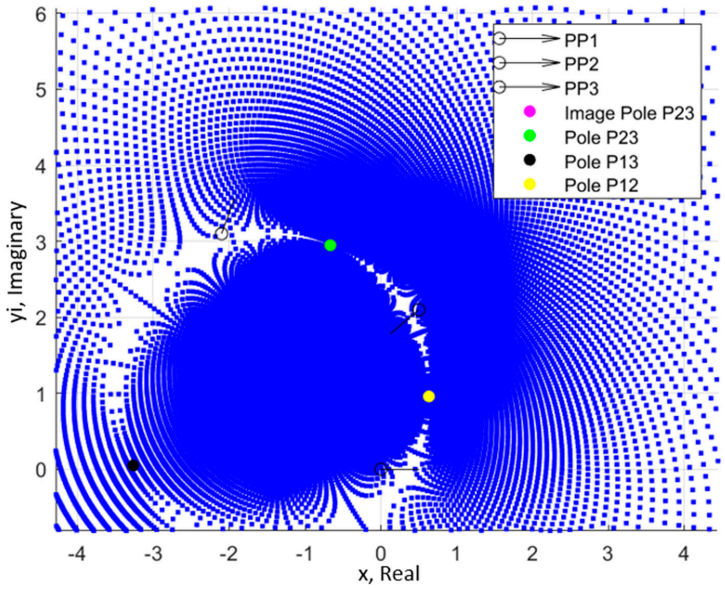


Figure 5. The solution density after shifting the position (+2 to the right) and angle (+180°) of the prescribed position 2.

Figure 2 shows the effect of positional density around a circle, indicating that the input free-choice values most frequently yield solutions near the pole locations. This effect is so dramatic that a 20° increment covers over 2/3rds (~70%) of the corresponding circle. But, this is only one portion of density's effect—there is a second dimension to the concept of solution density. That second dimension is the space between two adjacent circles. Along a single circle, as the angle increment of β_2 approaches 0, the circle of discrete points approaches a straight line. In the same way, as the increment between two circles approaches 0, the space between becomes a continuous surface of varying density. Once again, though, plotting multiple circles reveals that this dimension of solution density is greatest near the poles. This phenomenon may be observed in Figure 6, which is a recreation of Figure 5, but this time, the plot is created using a set of circles drawn as a single continuous line rather than a collection of individual points.

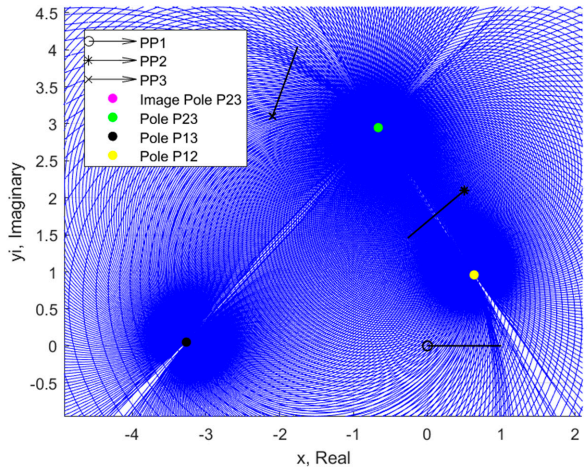


Figure 6. This figure is identical to Figure 5, but the solutions are plotted as single-line circles rather than a collection of points, providing a bit more clarity in how the circles form about the poles.

It is known from geometry (see Figure A2) that each circle passes through two of the poles exactly. The circle radius is set by the internal angle between the poles and center point, which is a factor of the free choices. The circle radius sets the second dimension of

solution density, a property that is even more obvious in Figure 7, which shows a single set of circles. The focus of the present work is on dyad chains, but some preliminary work of a similar nature has been conducted on triad chains as well. This foundational effort for future work to build off for triad chains is shown in Appendix C.

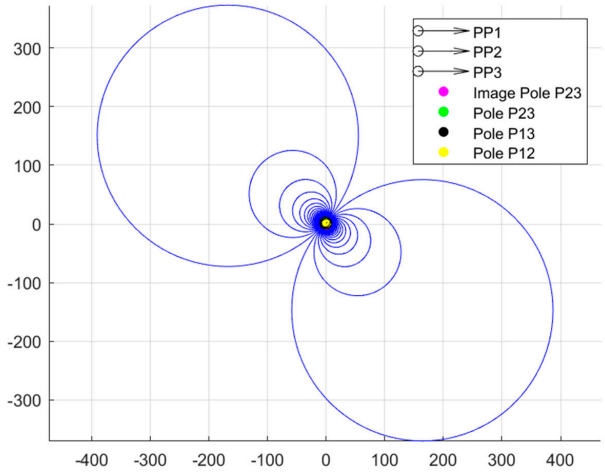


Figure 7. A zoomed-out view of the problem situation with only one set of circles shown. Here, each circle represents a new value of β_2, and the points on the circles are values of β_3. The space between each circle is iterated in 2° increments of the variable β_2 from 0 to 360, non-inclusive.

3. Applications to Mechanism Synthesis

A common tactic for finding solutions in mechanism synthesis is to apply a grid search over a set variable range. In a three-prescribed-position motion generation problem, a designer will often vary the values of the angles β_2 and β_3, with the solution yielding a single complete dyad. To make a complete four-bar, the first dyad is combined with a second dyad formed from another unique combination of β_2 and β_3. Testing 360 values for both β_2 and β_3 yields 129,600 unique dyads, and every resulting four-bar solution combines two of these kinematic chains into one mechanism. That means between just these two dyads, using one-degree increments, a designer will end up sifting through more than $8.398 * 10^9$ possible solutions (1).

$$\frac{129600 * 129599}{2} = 8.398 * 10^9 \quad (1)$$

Even with modern computing power, running that volume of solutions through a grid search (synthesizing solutions) and an affiliated optimization routine (finding ground pivots, mechanical advantage, velocity/acceleration analysis, transmission angles, etc.) will be a time-consuming and computationally expensive process. And that is only for a four-bar mechanism on a 1° increment! The complexity and volume of free choices further increase for mechanisms with more links. Even so, despite the astronomical number of solutions considered, the concept of solution density reveals that one-degree increments may not be a tight enough resolution. Figure 7 shows that even a small increment of β_2 can produce solutions hundreds of units apart. If a designer first creates a plot of the solution space or even just identifies the locations of the critical poles, they may use a larger increment of the free choices as the spacing between points is much tighter. The result is that designers sift through significantly fewer candidates on the way to their answer.

Manipulating the problem definition to improve solution density is valuable for finding solutions, but the impact of this concept extends beyond the theoretical to the practical construction of the mechanism. Figure 2a shows that the regions of high solution density contain essentially a single 'family' of solutions. All the dyads in this region

have the same general form, but slightly different dimensions. The opposite is true for the low-density solutions shown in Figure 2b, which have notably different geometries and dimensions. The result is that mechanisms designed with prescribed timing on the driving link will have more significant output inaccuracies at each set position of the input as solution density decreases. An equal change in angle β_2 or β_3 will produce a greater change in corresponding pivot locations in low-density regions than in high-density regions. Quantifying this output inaccuracy or identifying the amount tolerances must be tightened to accommodate solutions selected from low-density positions is not the emphasis of the present work. As shown in Figures 8 and 9, the change in density along each dimension changes non-linearly with respect to changes in the free-choice angles. Much of this effort, including comparing Faik's sensitivity study to the current study to identify correlations, is left for future work [51,55].

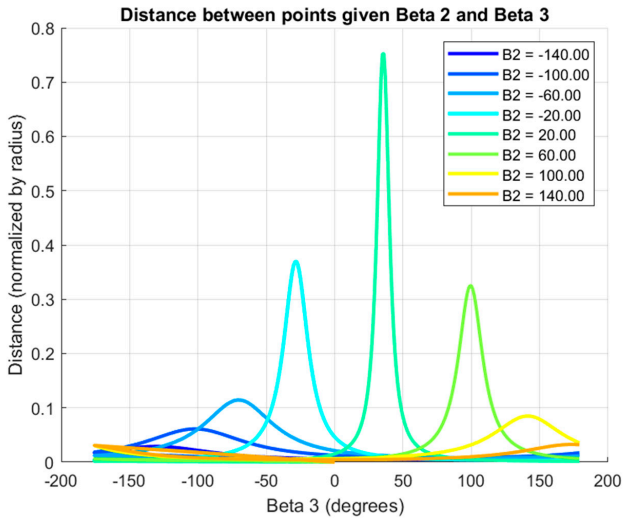


Figure 8. A plot of the linear distance between two adjacent points on an M circle given 4 different β_2 values. The magnitudes are normalized by the radius of each circle.

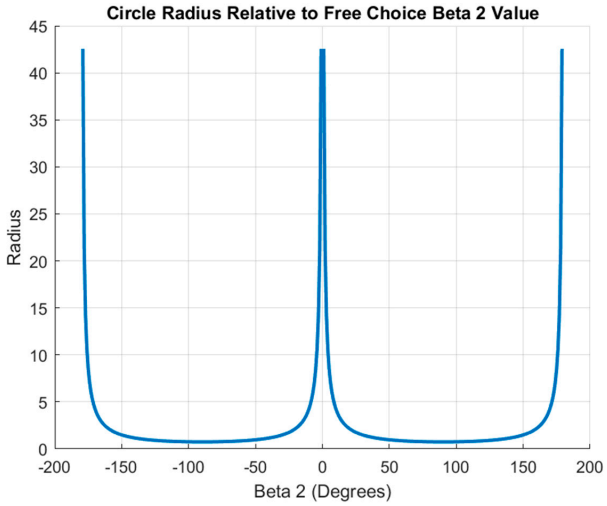


Figure 9. The radius of the M circle for many different values of β_2. This plot demonstrates an intuitive fact that as the interior angles of the circle approach a flat line between the poles, the diameter of the circle changes rapidly. This is true for angles of 180 degrees or angles of 0 degrees, creating the bowl-shaped curves shown in the plot. The value at these extremes is technically infinite, creating a slider point (also concurrency), which yields the asymptotic relationship shown in the plot.

The geometric construction procedure for each set of solutions found using the MK circles also reveals interesting information about how solutions fall in the plane. If β_2 and α_2 have opposite signs, the ground and moving pivot solutions will typically fall on the same side of pole P_{12}, while matching signs will lead to solution positions on opposite sides of pole P_{12} [8]. This is not necessarily significant for link lengths, but it is important for how links move, affecting instant centers, transmission angles, and other force transmission properties.

Figure 8 shows the density relationship between two adjacent points on any given circle. This relationship is governed by Equation (2), which finds the distance between two adjacent ground pivot solutions. The circles are continuous, so the distance will be dependent on the amount by which β_3 is incremented.

$$\text{Distance} = \sqrt{\text{Real}(M_1 - M_2)^2 + \text{Imag}(M_1 - M_2)^2} \tag{2}$$

where M_1 is ground pivot solution one, given by $PP1 - \mathbf{Z_1} - \mathbf{W_1}$, and M_2 is ground pivot solution two, given by $PP1 - \mathbf{Z_2} - \mathbf{W_2}$. For cases like the 3-position problem considered in Figure 8, **W** and **Z** may be calculated using Cramer's rule (Equation (3)), a method for solving a system of equations. In the example, to find $\mathbf{Z_2}$ and $\mathbf{W_2}$, the value of β_3 is incremented by 1°.

$$\boldsymbol{W} = \frac{\begin{vmatrix} \boldsymbol{\delta_2} & e^{i\alpha_2} - 1 \\ \boldsymbol{\delta_3} & e^{i\alpha_3} - 1 \end{vmatrix}}{\begin{vmatrix} e^{i\beta_2} - 1 & e^{i\alpha_2} - 1 \\ e^{i\beta_3} - 1 & e^{i\alpha_3} - 1 \end{vmatrix}}, \quad \boldsymbol{Z} = \frac{\begin{vmatrix} e^{i\beta_2} - 1 & \boldsymbol{\delta_2} \\ e^{i\beta_3} - 1 & \boldsymbol{\delta_3} \end{vmatrix}}{\begin{vmatrix} e^{i\beta_2} - 1 & e^{i\alpha_2} - 1 \\ e^{i\beta_3} - 1 & e^{i\alpha_3} - 1 \end{vmatrix}} \tag{3}$$

Figure 9 shows the effect of solution density between two circles. In that case, the density is a result of the radius of the circles, a property which is again a function of the free-choice angles. The radius may be calculated according to the geometry of the solution space, especially the pole locations. See Figure A2 for an example of the formulation. The result is shown in Equation (4), which simply applies trigonometric identities to the geometry to find the radius. Note that the equations for calculating the pole locations are provided in Table 1.

$$r = \left| \frac{\sqrt{Real(P_{13} - P_{23})^2 + Imag(P_{13} - P_{23})^2}}{2sin\beta_2} \right| \tag{4}$$

Equations (2) and (4) specifically relate to the ground pivot circles, but similar relationships exist for the moving pivot circles as well. The distance equation may be updated by replacing M with K, the moving pivot position, which is only a function of PP1 and **Z** rather than **Z** and **W**.

4. Solution Density Technique Applied to Chest-Style Coffee-Table Mechanism

A common challenge in mechanism synthesis is designing parallel (not rotating) or straight-line motion. Consider a common chest-style coffee table that opens from the top with a single hinge. If the user has anything on top of the table, it will need to be picked up and placed off to the side to access the contents of the chest, or else the items would slide off the top when the lid is opened. If the lid were instead mounted with a parallel-motion linkage that keeps the top surface flat as the lid moves up and out of the way, the items could be left in place even while the user accesses the chest. The simplest method

for creating parallel motion is to use a parallelogram four-bar linkage, but this design is known to suffer from poor mechanical advantage and takes up a large space relative to the travel distance of the parallel link. An alternative method is to generate a cognate 7-bar linkage using the Roberts-Chebyshev theorem [8,56]. In this method, two four-bar cognate linkages that generate an identical path to the base four-bar are created using geometric properties of linkages. If one of the cognates and the original linkage is then joined together, their shared paths create parallel motion. By Gruebler's equation, the final 7-bar linkage technically has 0-DOF ($F = 3\,(7-1) - 2 * 9 = 0$), but the presence of parallel motion allows the system to move nonetheless—taking away the constant angle bar between the two four-bar segments does not change the motion of the mechanism. See Appendix B for a more complete description of the Chebyshev theorem, and instructions for applying it.

Conveniently, these properties make the theorem conducive to solution density optimization, as the base linkages produce parallel motion regardless of the values of α_j. In the following example, solution density optimization and the Chebyshev theorem are used in tandem to synthesize a parallel-motion generator for use inside a coffee table that has an internal height of 12 inches and an in-plane width of 15 inches. The goal is to create a parallel-motion linkage that allows a user to open a coffee table and access its contents without needing to remove anything sitting on top of it. The problem definition is initially set using the parameters in Table 3. The ground pivots must be positioned underneath the prescribed positions (and ideally a bit to the left), so the alpha values are adjusted to those shown in column α_b from α_a after observing the solution density plots shown in Figure 10A,B. To adjust the problem, the designer may either use the equations shown in Table 1 to directly find favorable values of δ_j and α_j, or simply guess at ideal values and replot the poles until they are satisfied.

Table 3. Prescribed position data defining the problem.

Position	δ (in)	α_a	α_b
2	0.5 + 4i	40	−45
3	10 + 3i	70	−90

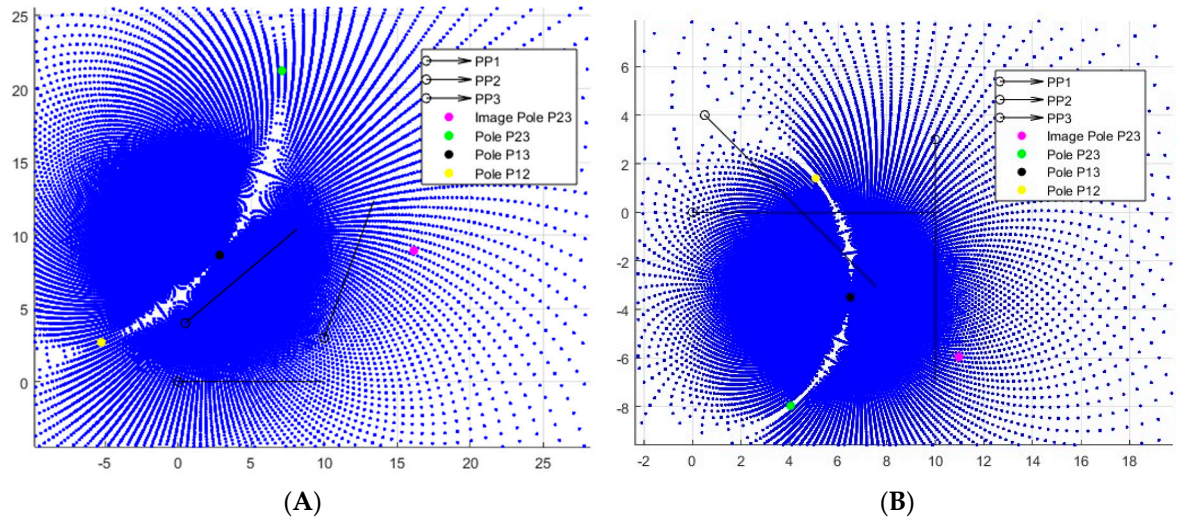


Figure 10. Comparing the ground pivot solution density for (**A**) the initial problem definition δ_j and α_j, and (**B**) the optimized problem definition δ_j and α_j. In (**B**), the densest region of ground pivot solutions has shifted below the prescribed positions, meaning they are in the ideal location inside the coffee table. All units are in inches.

In this example, the criteria for a solution to be considered 'passing' are the following:

1. The ground pivots for dyads A and B of the base four-bar linkage must be inside the compartment of the coffee table. This range is selected as $-3 < O_{ax} < 12$ in the X-direction, and $-12 < O_{ay} < 0$ in the Y-direction. Both ranges are set relative to the first prescribed position in which the coffee table is fully closed.
2. The maximum length of a link does not exceed 6 inches. After analyzing a few preliminary solutions, it became clear that in a seven-bar mechanism, the links would almost certainly strike the side walls of the container if they were too long. As a result, this limit is initially set low at 6, with the opportunity to relax it to 8–10 inches if no solutions are found. *
3. In the first (closed) position, the moving pivots also must be contained within the bounds of the coffee table. These limits are the same as the first set.
4. The final requirement is to reapply criteria 1–3 to the synthesized cognates generated from the base four-bar linkages. For the sake of efficiency, the left and right cognates are not generated unless the base four-bar passes the first three criteria.

* Note that the link length filter applied in step 2 is a specific criterion tied to the application's requirement that a large mechanism operate in a tightly confined space. This filter could easily be replaced or combined with any other filter examining a linkage property, like mechanical advantage at a position or average transmission angle. It would also be trivial to add a "sorting" filter after this step that does not reject any possible designs but organizes the list of solutions in order of a quantifiable performance metric like maximum link length or mechanical advantage.

The flow chart shown in Figure 11 summarizes the synthesis procedure.

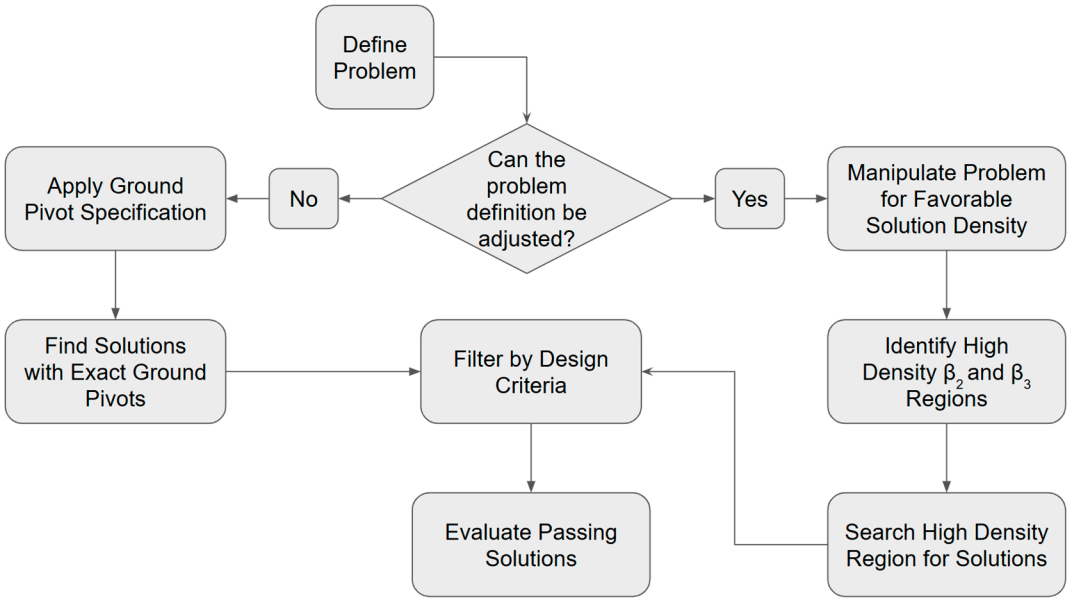


Figure 11. Synthesis Process for Finding Solutions by Optimal Solution Density.

Specifying the location of a ground pivot is a common problem in linkage synthesis, but setting the location of moving pivots is a similarly important, but less well-studied, task in kinematics. For the case of an internal hinge, like the one designed here that must reside entirely inside the coffee table in the first position, it is significant to verify that the moving pivots are in an appropriate location. To this end, Figure 12 is generated, which shows the solution density map of the moving pivot locations in the first position. The figure confirms that there is a high density of moving pivot solutions inside the region defined as the inside of the table, increasing the odds of finding solutions.

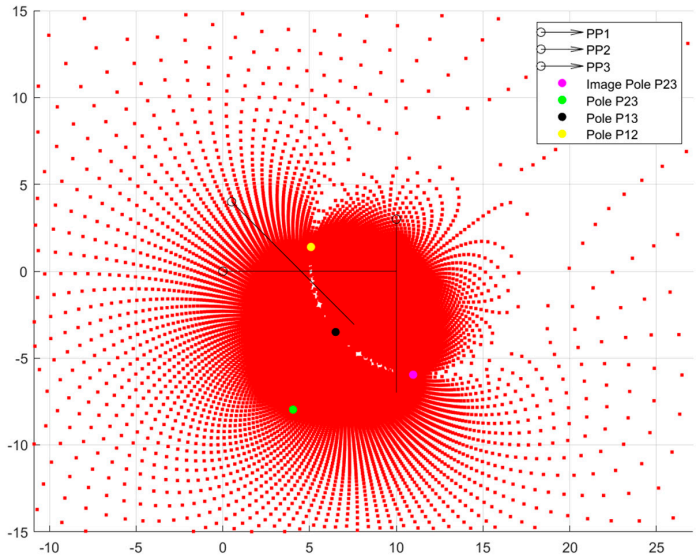


Figure 12. The moving pivot solution density map, like the ground pivot map, has its highest solution density region underneath the prescribed positions, ideally positioned inside the coffee table. All units are in inches.

Using the listed criteria to filter solutions, a reduced-scale grid search is applied. β_{2a} and β_{2b} are varied from $-90°$ to $90°$ in $5°$ increments, while β_{3a} and β_{3b} are varied from $-180°$ to $180°$ in $10°$ increments. This script takes less than 30s to run in MATLAB using version R2020b. In the α_b configuration of Table 3—533 solutions pass the selection criteria on the search over the four beta values, totaling 1.67 million options tested (0.032% success). To put this in perspective, the same search algorithm operating over the α_a problem definition resulted in 0 passing solutions. If the maximum link length is expanded to 8 inches, 135 solutions pass the criteria (applying the same relaxation to the B configuration results in 52669 passing solutions, which is 0.008% passing on A and 3.154% on B). Not every one of these solutions found using the A configuration was specifically examined, but the majority ultimately fails because they are too wide, or the links pass through the top lid of the container at some point during the motion. For additional comparison, if the same script is set with the A configuration and runs with a $1°$ increment on each variable, it is estimated to take 150+ hours to complete. It is unknown how many solutions this version of the script produces because it was not feasible to complete the analysis. One of the identified solutions from the B configuration is analyzed in greater depth. The synthesized values that make up this linkage are shown in Table 4.

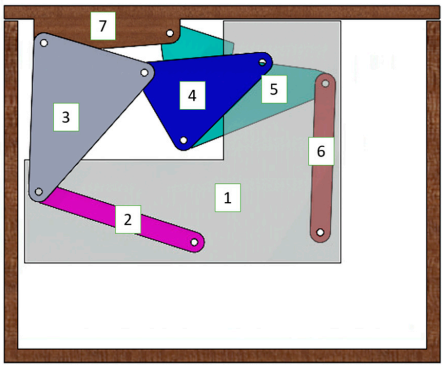
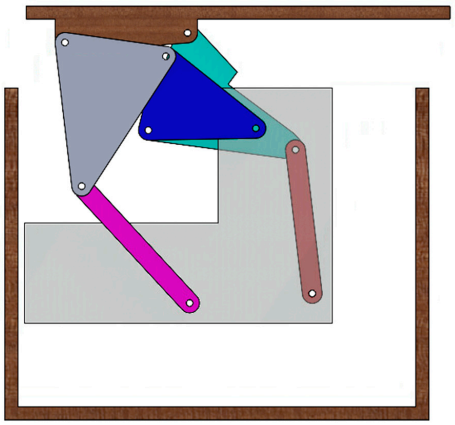
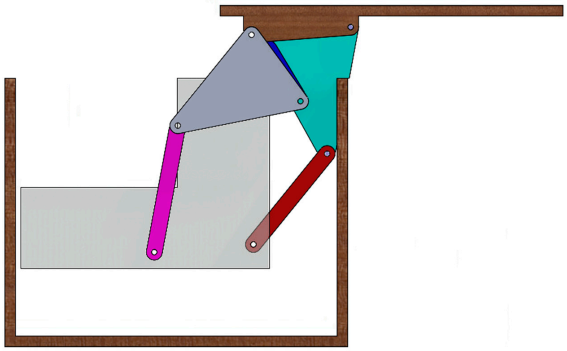
Table 4. Candidate Coffee-Table Linkage Solution Parameters.

Variable	**Dyad A (Red-Cyan)**	**Dyad B (Blue-Cyan)**
Beta 2	0.3491, (20°)	−1.3265 (−75°)
Beta 3	−0.6981, (−40°)	2.4435 (140°)
W	1.1742 + 5.3225i (in)	−1.5132 − 3.7672i (in)
Z	−5.9267 + 0.9268i (in)	−1.1129 + 3.7932i (in)
	Cognate Vector Value (in) *	
CI *	−3.8216 − 2.0712i	
IP	−3.4307 + 1.7377i	
FP	1.1742 + 5.3225i	
M_1F	−5.9267 + 0.9268i	

* See Appendix B for the layout of cognate vectors.

The MATLAB figure portraying the synthesized solution of Table 4 is visualized moving through the three prescribed positions in Figure 13. A CAD rendering of what a physical version of the mechanism might look like is shown in Table 5. The primary goal in providing this example is to quantitatively demonstrate the impact of optimizing solution density as an intentional, isolated step in the kinematic synthesis procedure with a relative comparison to the performance of a blind grid search. Even so, a preliminary analysis and discussion of the kinematic properties of the selected solution are provided below.

Table 5. The solution mechanism is practically represented in the SolidWorks 2024 CAD software.

Position	CAD Rendering of This Position
PP1 In the first position, the lid of the coffee table is tightly closed and the mechanism is folded up entirely inside the table.	
PP2 In the second position, the tabletop moves mostly vertically upward with a slight translation to the right.	
PP3 The notch added to the cyan ternary link meshes with the edge of the coffee table to provide increased stability while resting at the third position. The contents of the chest are accessible.	

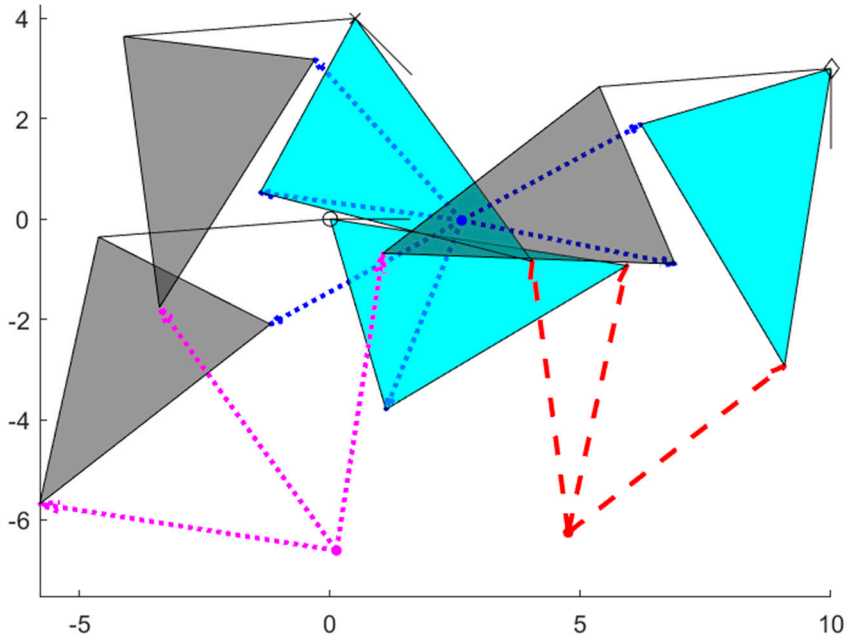


Figure 13. The output of the MATLAB script visualizing the position of each link in 3 positions. All axes' units are in inches. The link colors correspond to the colors shown in Table 5. The red and cyan links are formed by the first dyad, while the dark blue are second leg of the cyan link are formed by the second dyad. The magenta link corresponds to vector M_1F in Table 4. FP and IP form the gray triangle, and the second vector of the dark blue link corresponds to CI. See Appendix B for a full vector layout.

Two modes of driving the mechanism are considered. First, a user could grab directly onto the tabletop, presumably at the front edge (consider Table 5). Alternatively, an internal motor, either a rotary motor or a linear actuator, could apply an internal force to move the mechanism. For this second option, three primary links are considered as possible driving links. Links 2, 4, and 5 rotate in a single direction, making them well-suited to driving the mechanism. Links that rotate in a single direction throughout the full range of motion reduce ambiguity, as at the inflection point when the motor starts turning back in the other direction, it is uncertain whether the mechanism will continue forward or turn back. Of the three links, 2 and 4 are both connected to ground, making it easier to mount a motor to drive them directly without some form of geared setup.

If the tabletop is driven directly, the user will be exerting a torque and lateral force, but the link is not rotating, so the torque will be largely distributed along the link into the ground pivots. One good indicator of how efficiently force is transmitted through the mechanism is the transmission angle. This angle is most ideal at 90°, but performance typically remains quite good at ranges above 65°. Notably, 30° is commonly chosen as the minimum value below which the mechanism cannot function reliably. The velocity direction of link 7 is determined using the instant center approach in position 1. In Figure 14, note that the instant center (1,7) is an infinite line (like a slider) because the link is not rotating. Here, the transmission angle between a vertical force $\mathbf{F_{in}}$ and the tabletop link velocity $\mathbf{V_7}$ is 74°. Repeating this same method at positions 2 and 3, the transmission angles are 50° and 49°, respectively. The instant center calculations for positions 2 and 3 are shown in Figure A4. Note that just after position 2, it is assumed the operator switches from applying a vertical upward force to a horizontal force—this force application should feel natural, matching the up and back motion of the tabletop.

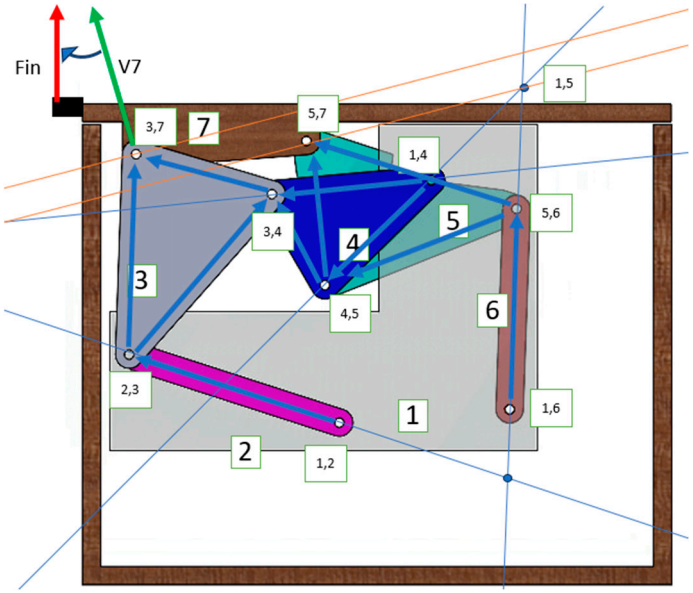


Figure 14. The figure shows the instant center velocity direction analysis of link 7. The non-existence of the instant center (1,7) confirms that link 7 has no rotational velocity in this position. Like a slider, the velocity of the link at this position is perpendicular to the infinite slider axis. The numbers in the figure represent the link numbers (used only for referencing purposes) and the location of the instant centers.

If the linkage is driven by a motor instead of directly grabbing the tabletop, it is important to verify that the motor can transmit power throughout the linkage in the entire range of motion. Examining the case where link 2 is driving the mechanism, unfortunately, this results in a position where the transmission angle between links 2 and 4 reaches 0° between positions 2 and 3, as shown in Figure 15. If a different link is driven for the remainder of the motion, link 2 remains motionless after reaching this position. That makes relying on link 2 as the sole driver of the system impossible.

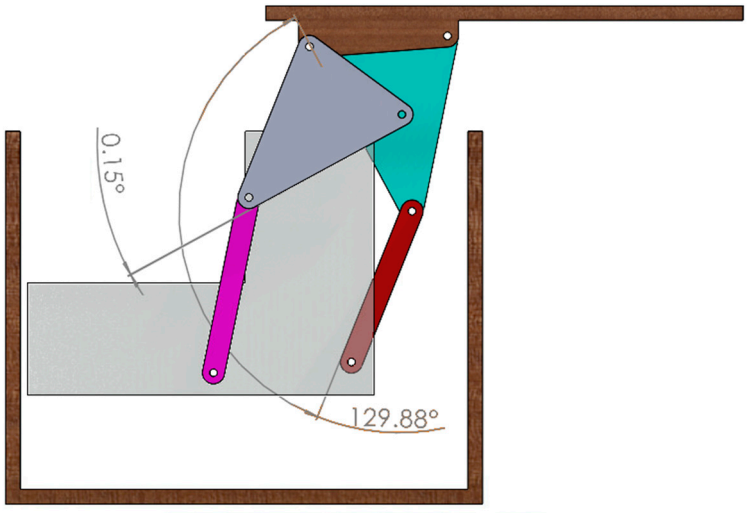


Figure 15. The transmission angle between links 2 (magenta) and 4 (dark blue) reaches 0 at this point in the motion between positions 2 and 3, making driving link 2 an ineffective choice.

If instead the user drives link 4, an interesting property of the cognate parallel-motion linkage is observed—the transmission angles on either side of the central link are always the same. Throughout the motion, the angles are generally quite good, with the single

exception shown in Figure 16, where the transmission angles dip down to 32°. Although this is technically above the 30° threshold, these low angles are still a warning sign for the mechanism's motion. Fortunately, they occur when the tabletop is near its peak height, hopefully mitigating the losses from lifting against gravity with poor force transmission.

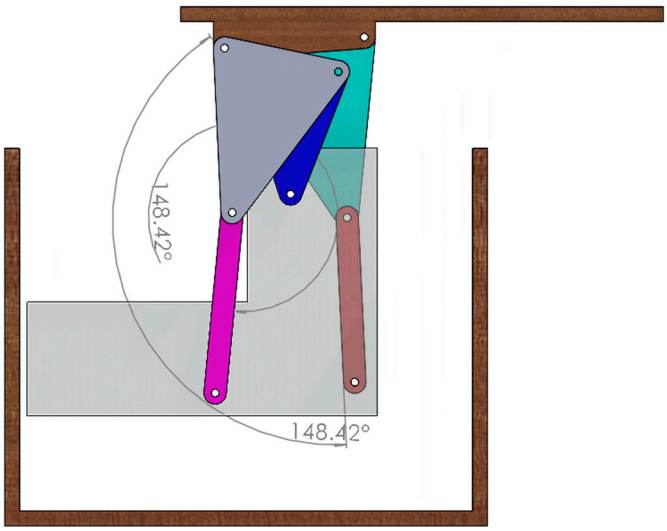


Figure 16. Minimum transmission angle throughout the motion when driving link 4.

A middle-ground option may be to drive the linkage by driving the tabletop directly, but to add an internal torsion or linear spring to assist the user in actuating the linkage. This would make the tabletop feel lighter during the lift between positions 1 and 2 and would help keep the tabletop in the open position until the user intentionally pulls it closed. This option will also be cheaper/easier to manufacture than a motorized version.

5. Advantages and Limitations of the Proposed Technique

The method of optimizing solution density is demonstrably effective in generating more solutions to a given problem when testing an equal number of candidate values (a higher percentage of synthesized links pass design requirements). For completeness, it is important to emphasize that the proposed technique is not based on new dimensional synthesis equations. The underlying math is identical to the MK circle method, an approach based on solving the synthesis equations with linear algebra. Rather, optimizing solution density is an optional added step in the normal workflow for any exact or mixed exact-approximate synthesis problem. Once learned, this technique only takes a few minutes to implement in a new problem and guarantees a high volume of solutions with ground and/or moving pivots in favorable regions. The core advantages of the technique are that it increases the probability of finding a good solution (in the case of the coffee-table example, applying the technique increased the number of solutions from 0 to 533 on a search of 1.67 million options) and increases a designer's understanding of the solution space. There is no guarantee that this approach will yield better linkage solutions—rather, the intent is to encourage designers to integrate this novel, intuitive step into their existing planar linkage synthesis workflow, saving time overall and improving the quality and consistency of the synthesis process.

With these benefits in mind, it is worth noting some of the limitations of the approach and identifying areas for future work. First, the method of optimizing solution density does not guarantee that the synthesized linkages will have favorable properties (transmission angle, mechanical advantage, etc.). Rather, the focus is on ensuring there are solutions to the prescribed problem while minimizing the computational load required to find them.

With that said, optimizing solution density does tend to increase the probability of finding favorable solutions. As shown in the practical example, an optimized problem yields more solutions over the same search depth, and solutions tend to have shorter link lengths. There are exceptions, especially in cases where α_2, α_3, or α_{23} are nearly 0 (slider point), or the case where $\alpha = \beta$ (concurrency point). In these cases, the poles are infinitely far away, increasing the length of the links unless they are fully replaced with sliders. Shorter links are favorable for designers hoping to manufacture the synthesized mechanism or fit it in a confined space, and short output links are often associated with high mechanical advantage.

Another limitation is that applying this method is dependent on having some degree of flexibility in the problem definition, either in the positions (δ), the angles (α), or ideally, both. If a problem definition is truly inflexible and each position must be reached exactly, a different synthesis approach must be applied. Similarly, this method is most effective when applied to problems with ideal ground pivot regions, rather than singular ideal ground pivot points. In the case where an exact ground pivot position is required, the designer may use the method of exact ground pivot specification.

6. Conclusions and Future Work

This paper has presented the foundations of linkage synthesis aided by optimized solution density. The method allows a user to manipulate their problem parameters, creating a configuration that ensures a high volume of solutions with pivot locations in the prescribed region. The method is demonstrably effective in identifying a greater number of solutions at equal search depth, and in many cases, like the one provided here, those solutions also exhibit better properties than the alternatives. With this foundation in place, there remain several opportunities for future work. The first is to expand the approach to also apply to triad chains, not just dyads. For most synthesis methods, adapting to triads only requires expanding the standard form equations to accommodate an additional vector. In this case, the process is a bit more involved. The same basic solution density plot can be generated (example shown in Figure A7), but interpreting the figure is not as simple as the dyad plot. Some preliminary work on this topic has been completed and is shown in Appendix C, but the majority of the effort is left for future work.

Another opportunity for future work is identifying explicit equations for how the density varies relative to position in the plane rather than just the free-choice variables. An equation of this form would be valuable for numerically representing the density. Examining the plots makes it clear to see how solution density varies in the plane. Still, it would be beneficial to know the solution density properties of the plane more exactly without needing to plot the solutions. A general equation for either (or both) primary directions would also just be valuable in deepening our understanding of the dyad solution space.

A few more areas for future work are in representing and plotting the density information. Plotting individual pivot points is reasonably effective in demonstrating where density is highest, as shown in this paper. However, in the highest density regions, the points get so close together that they look like a continuous mass rather than discrete points. That makes it difficult to differentiate the true highest density position from a general high-density region. What might be more effective is to use a heat map plotting style that uses color to represent the third dimension, density, in a 2D plot. The challenge with setting up this type of plot is that the density quantity varies non-linearly in multiple dimensions, and without explicit equations for the density in each of these dimensions related to their position in the plane, the overall density is difficult to calculate. This task is left to future research. A similar objective is to create a density map that represents multiple moving pivot locations. In the example provided here, the position of the moving pivots is most

essential in the first position, as all links need to be contained inside the box. In other cases, though, like a mechanism moving through a confined space, it may be necessary to ensure that the moving pivots are within an acceptable region in all positions. Representing where the moving pivots will be in each position would also be valuable information to the designer.

Author Contributions: Conceptualization, S.M. and A.E.; Formal analysis, S.M.; Funding acquisition, A.E.; Methodology, A.E.; Project administration, A.E.; Resources, A.E.; Software, S.M.; Supervision, A.E.; Visualization, S.M.; Writing—original draft, S.M.; Writing—review & editing, A.E. All authors have read and agreed to the published version of the manuscript.

Funding: This research received no external funding.

Data Availability Statement: No new data were created or analyzed in this study. Data sharing is not applicable to this article.

Conflicts of Interest: The authors declare no conflict of interest.

Appendix A. Supplementary Figures

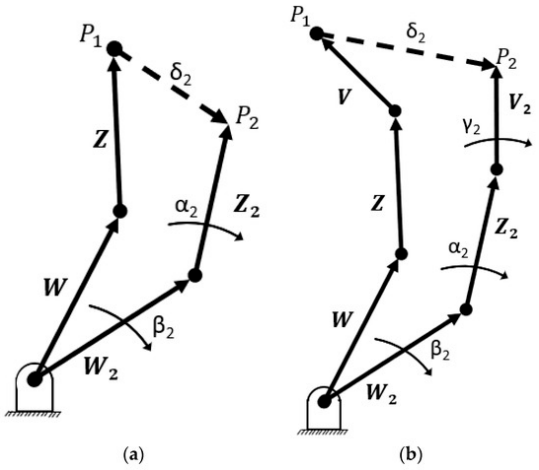


Figure A1. (**a**) The vector and angle notation for a two-link, dyad kinematic chain in two positions. (**b**) The vector and angle notation for a three-link, triad vector chain in two positions [47].

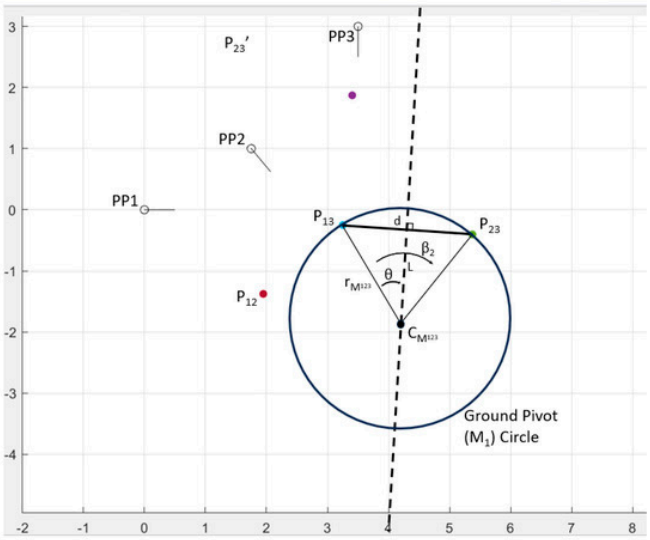


Figure A2. The derivation from geometry of one ground pivot (M) circle [47]. See References ([8,46,47]) for a full explanation of constructing the circles by geometry.

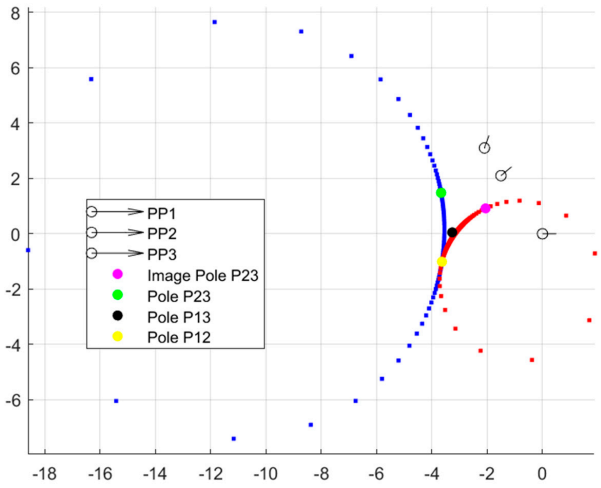


Figure A3. Solution density visualized for a fixed value of β_3, and iterating values of β_2 (opposite of Figure 1). P_{13} is no longer a point that both circles pass through (now P_{12} is shared), but the solution density is still much higher around the pole locations.

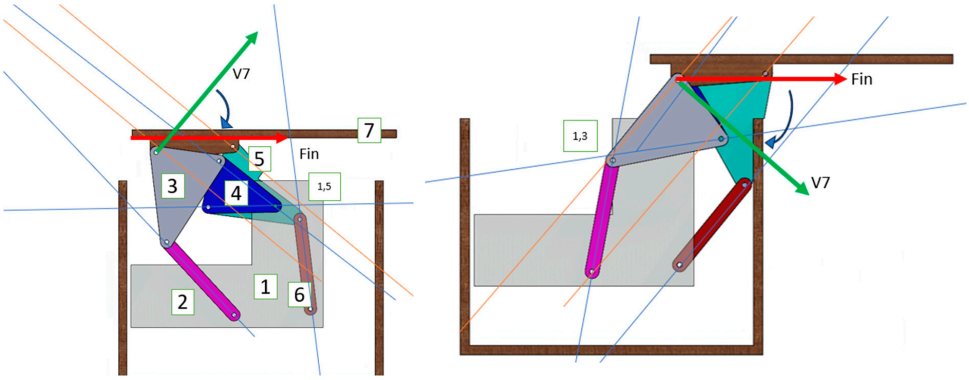


Figure A4. The instant center calculations to find velocity direction V_7 in the 2nd and 3rd positions. Note that the instant center (1,7), indicated by the intersection of the parallel orange lines, is infinitely far away. This proves that in each position, link 7 is not rotating.

Appendix B. Roberts-Chebyshev Theorem Explanation

The Roberts-Chebyshev Cognate Theorem is a useful tool for designers that allows the exact geometric replication of the path of a particular four-bar linkage. Every four-bar has two geometric cognates that are guaranteed to reproduce the same tracer-point path, though not the same motion, as the base mechanism used to generate them. To identify the cognates, the designer forms a series of parallelograms about the base four-bar, as well as using the mathematical rule of similar triangles to set dimensions. An example of the construction is shown in Figure A5.

In Figure A5, parallelogram M_1-F-P-A is formed by replicating the chain W_1-Z_1 but switching the order of these two vectors. Z_1' extends from M_1, and W_1' starts at the distal end of Z_1'. The same relationships are used from M_2 with vectors W_2 and Z_2. With these parallelograms in place, three similar triangles are created. Each of these triangles is similar to APB. The first is used to find point C using triangle M_1CM_2, which, again, is similar to the coupler link. The other two similar triangles form the coupling links of the two cognates, FIP and PHG. To finalize the two cognates, points I and H are connected to the newly identified ground pivot C. As a function of their geometry, each of these cognates exactly reproduces the path of the point P of the base four-bar.

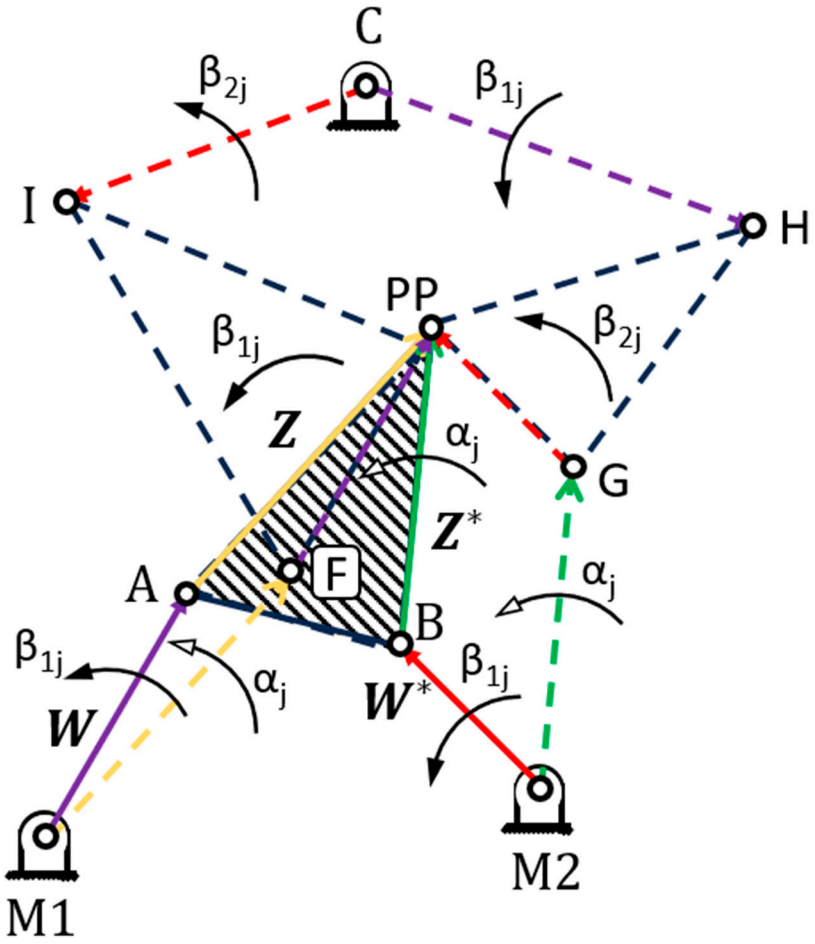


Figure A5. Example of the construction of the left and right cognates of a four-bar. Here, links CI, IPF, M_1F, and ground M_1C form one cognate. Links CH, HPG, M_2G, and ground M_2C form the other cognate. Links M_1A, APB, M_2B, and ground M_1M_2 form the base four-bar linkage. APB, M_1CM2, FIP, and PHG are all similar triangles.

To convert the cognates into a parallel-motion generating 7-bar linkage, their relative position must be shifted. Take note of the angular relationships that propagate through the cognate linkages. Any time a vector quantity is copied in a parallelogram (e.g., M_1F is a shifted copy of Z_1), the copied vector also inherits the prescribed rotation angles of the vector in the base four-bar (M_1F rotates by α_j just like Z_1). Similarly, all vectors embedded in a triangular link must rotate by the same amount because the link is assumed to be rigid. Between these two properties, if the rotations of the base four-bar are known, the rotations of all links in the generated cognate linkages are also known. This is important to note, as creating parallel motion requires not just that the cognate reproduces the same path as the base four-bar, but also that it reproduces that path at the same speed. If the base four-bar moves an inch, the tracer point of the cognate must also move an inch in the same direction—if it does not, the link will rotate or deform.

Due to the angular relationships that propagate through the linkage and cognates, it is possible to shift the position of the cognate and fuse two links together to create a larger, 6-bar parallel-motion generator. Notice in Figure A5 that the links CI and M_2B both rotate by β_{2j} between each prescribed position. As a result, it is possible to shift the left cognate chain (C-I-F-M_1) down so that C is at the same point as M_2. Then, if the links CI and M_2B are fused into a single link M_2IB, their shared rotation guarantees that the tracer points of the base four-bar and the cognate linkage will move identically in the plane. The result is that if a seventh link is added, connected between the tracer points of the two four-bars, it

will not rotate, no matter how the other links in the mechanism are moved. Normally, the addition of this seventh link would result in a structure, but thanks to the parallel-motion property, the mechanism still moves even though it technically has zero degrees of freedom. The completed parallel-motion generator after the shift is shown in Figure A6.

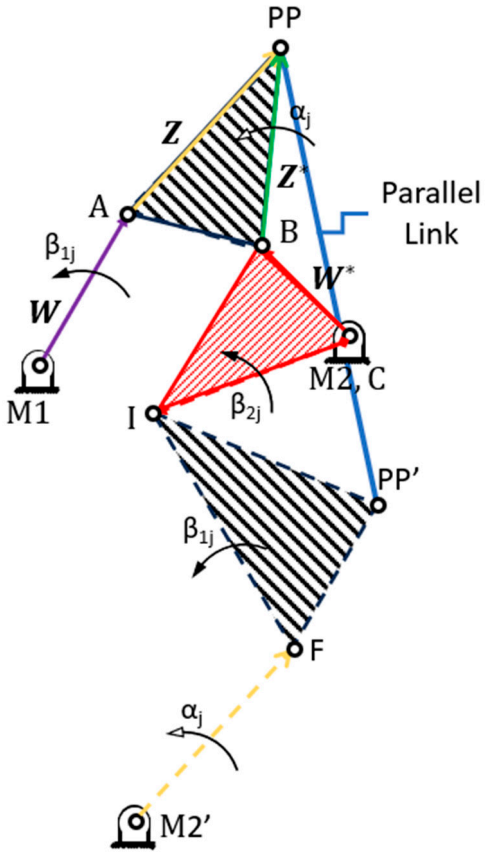


Figure A6. A generic seven-bar parallel-motion generator created using the Roberts-Chebyshev Theorem. As a property of the special geometry of this linkage, the link labeled "parallel link" does not rotate regardless of how the other links in the mechanism move. Note that the base topology here is a Watt II six-bar linkage, with the key difference being the additional link strung between the two path tracer points.

Appendix C. Solution Density Application for Triads

This paper emphasized applying solution density to dyad chains, but the fundamental ideas of the technique are also applicable to other kinematic chains. Triad chains are known to form circles like dyads (MKT circles—there are three circles per set corresponding to the three links of the chain [47]). Figure A7 shows one example of the ground pivot solutions for a triad chain in two cases. The problem situation is the same as the chest-style coffee table given in the body of the paper, though a fourth position has been added at the end of the motion. All three β angles are iterated from 0 to 360, though in large degree increments to avoid over-cluttering the figures. As was the case in Figure 10, manipulating the problem definition (in this instance both the α and γ angles, not just α) results in a dramatic shift in the location of the high-density region. Again, the new angles are intentionally selected to shift the high-density region below the prescribed positions into the empty space inside the coffee table.

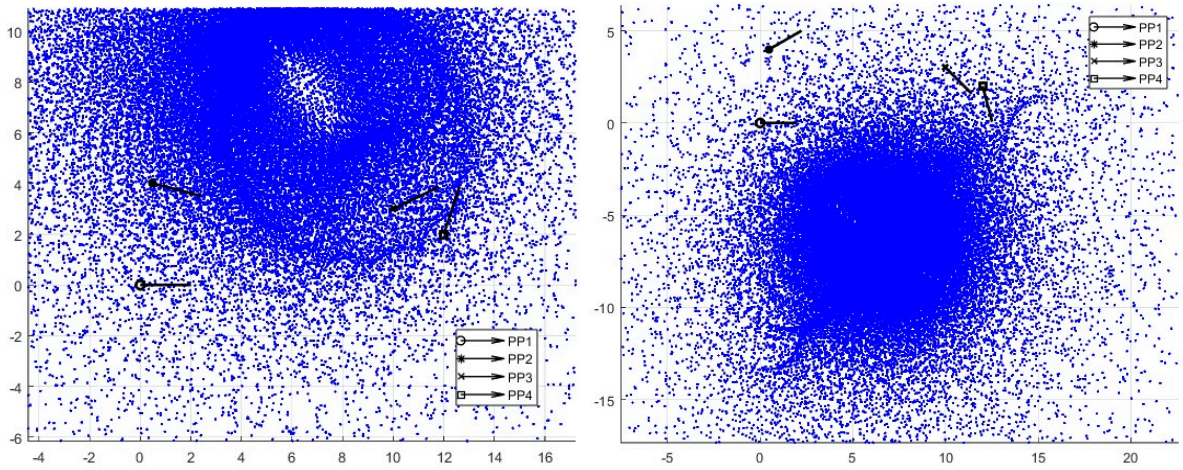


Figure A7. Comparing the ground pivot solution density for (**A**) the initial problem definition δ_j and α_j, and (**B**) the optimized problem definition δ_j and α_j. The full problem definition is given in Table A1. In (**B**), the densest region of ground pivot solutions has shifted below the prescribed positions, meaning they are in the ideal location inside the coffee table. All units are in inches.

Table A1. Triad Example Problem Definition.

Case/Angle	**(A) (°)**	**(B) (°)**
Beta β (initial values)	[0, 45, 20, 100]	[0, 45, 20, 100]
Alpha α	[0, −90, 43, 57]	[0, −45, −90, −55]
Gamma γ	[0, −45, 25.75, 71.62]	[0, 30, −45, −75]
Prescribed Positions	**(A) (Inches)**	**(B) (Inches)**
PP1	0 + 0i	0 + 0i
PP2	0.5 + 4i	0.5 + 4i
PP3	10 + 3i	10 + 3i
PP4	12 + 2i	12 + 2i

Although the situation shown in Figure A7 shows that the principles of solution density are applicable to triad chains just like dyads, a great deal of work remains to fully understand the triad solution space. Other than a few obvious special cases, like $\beta_j = \alpha_j = \gamma_j$, which yields the same solution as the dyad special case $\beta_j = \alpha_j$, the location of the triad poles has not been investigated. When synthesizing dyads, a designer can use the locations of the poles in the plane to predict how the MK circles are going to form, and consequently, the regions of highest density. Presently, while synthesizing triads, advanced knowledge of how the circles are going to form does not exist at a high enough level to adequately predict the behavior. As a result, designers are stuck generating plots like Figure A7 to understand the solution density, and that process will be much more time-consuming than simply manipulating the poles.

In addition to the challenges posed by the poles, optimizing the solution density of a triad chain is also more complicated than that of a dyad. Where the dyad has two angle sets to manipulate, β and α, the triad adds a third angle, γ. While this addition does make the problem quite a bit more complex, it also offers the designer an additional variable to control. It is no longer strictly necessary for either the α or γ angles to be adjustable, provided one of the two is. This added flexibility is promising for the solution density technique, possibly making it applicable in a broader range of circumstances. Overall, while

the principles of solution density are clearly applicable to triads, significant additional work is required to flesh out the method.

References

1. Willis, R. *Principles of Mechanism*; University of Cambridge: Cambridge, UK, 1841.
2. Reuleaux, F. *Lehrbuch der Kinematik*; F. Vieweg and Sohn: Braunschweig, Germany, 1875. Available online: https://archive.org/details/lehrbuchderkine01reulgoog (accessed on 21 March 2024).
3. Freudenstein, F. An Analytical Approach to the Design of Four-Link Mechanisms. *Trans. Am. Soc. Mech. Eng.* **1954**, *76*, 483–489. [CrossRef]
4. Freudenstein, F.; Sandor, G.N. On the Burmester Points of a Plane. *J. Appl. Mech.* **1961**, *28*, 41–49. [CrossRef]
5. Sandor, G.N. *A General Complex-Number Method for Plane Kinematic Synthesis with Applications*; Columbia University: New York, NY, USA, 1959. Available online: https://www.proquest.com/docview/301890904?Theses&fromopenview=true&pq-origsite=gscholar&sourcetype=Dissertations&parentSessionId=dN%2BPismefi0wSA%2BQ0FKllggl7tJm6zXBZQZC6oFTBxA%3D (accessed on 1 April 2024).
6. Hartenberg, R.S.; Denavit, J. *Kinematic Synthesis of Linkages (Mechanical Engineering Series)*; McGraw-Hill: New York, NY, USA, 1964.
7. Sandor, G.N.; Erdman, A.G. *Advanced Mechanism Design: Analysis and Synthesis Vol I*; Prentice Hall: Hoboken, NJ, USA, 1984; Volume 1.
8. Sandor, G.N.; Erdman, A.G. *Advanced Mechanism Design: Analysis and Synthesis Vol II*; Prentice Hall: Hoboken, NJ, USA, 1984; Volume 2.
9. Chase, T.R.; Erdman, A.G.; Riley, D.R. Triad Synthesis for up to Five Design Positions With Application to the Design of Arbitrary Planar Mechanisms. *J. Mech. Transm. Autom. Des.* **1987**, *109*, 426–434. [CrossRef]
10. Lin, C.-S. *Dimensional Synthesis of a Planar Triad for Six Precision Positions*; University of Minnesota: Twin Cities, MN, USA, 1987; p. 153.
11. Subbian, T.; Flugrad, D.R. Five Position Triad Synthesis With Applications to Four- and Six-Bar Mechanisms. *J. Mech. Des.* **1993**, *115*, 262–268. [CrossRef]
12. Soh, G.S.; McCarthy, J.M. The synthesis of six-bar linkages as constrained planar 3R chains. *Mech. Mach. Theory* **2008**, *43*, 160–170. [CrossRef]
13. Diab, N. Using Instantaneous Invariants of the Curvature Theory in Motion Generation Synthesis of 4R Mechanisms with Higher-Order Coupler Point Kinematics. *Mech. Mach. Theory* **2024**, *195*, 105596. [CrossRef]
14. Midha, A.; Zhao, Z.L. Synthesis of planar linkage via loop closure and nonlinear equations solution. *Mech. Mach. Theory* **1985**, *20*, 491–502. [CrossRef]
15. Holte, J.E.; Chase, T.R.; Erdman, A.G. Mixed Exact-Approximate Position Synthesis of Planar Mechanisms. *J. Mech. Des.* **2000**, *122*, 278–286. [CrossRef]
16. Sutherland, G.H. Mixed Exact-Approximate Planar Mechanism Position Synthesis. *J. Eng. Ind.* **1977**, *99*, 434–439. [CrossRef]
17. Zhao, P.; Ge, X.; Zi, B.; Ge, Q.J. Planar linkage synthesis for mixed exact and approximated motion realization via kinematic mapping. *J. Mech. Robot.* **2016**, *8*, 051004. [CrossRef]
18. Vasiliu, A.; Yannou, B. Dimensional synthesis of planar mechanisms using neural networks: Application to path generator linkages. *Mech. Mach. Theory* **2001**, *36*, 299–310. [CrossRef]
19. Zhang, C.; Norton, P.E.R.L.; Hammonds, T. Optimization of parameters for specified path generation using an atlas of coupler curves of geared five-bar linkages. *Mech. Mach. Theory* **1984**, *19*, 459–466. [CrossRef]
20. Tsai, L.W.; Lu, J.J. Coupler-Point-Curve Synthesis Using Homotopy Methods. *J. Mech. Des.* **1990**, *112*, 384–389. [CrossRef]
21. Diab, N.; Smaili, A. Optimum exact/approximate point synthesis of planar mechanisms. *Mech. Mach. Theory* **2008**, *43*, 1610–1624. [CrossRef]
22. Larochelle, P. Using Optimization for the Mixed Exact-Approximate Synthesis of Planar Mechanisms. In Proceedings of the 39th Mechanisms and Robotics Conference, Boston, MA, USA, 2–5 August 2015; Volume 5B, pp. 1–9.
23. Liu, W.; Qu, X.; Li, B.; Qin, T.; Sun, J. Dimensional synthesis of motion generation of a planar four-bar mechanism. *Mech. Based Des. Struct. Mach.* **2024**, *53*, 1201–1227. [CrossRef]
24. Fang, W.E. Simultaneous Type and Dimensional Synthesis of Mechanisms by Genetic Algorithms. In Proceedings of the ASME 1994 International Computers in Engineering Conference and Exhibition, Minneapolis, MN, USA, 11–14 September 1994; Volume Part F1678, pp. 35–41. [CrossRef]
25. Cabrera, J.A.; Simon, A.; Prado, M. Optimal synthesis of mechanisms with genetic algorithms. *Mech. Mach. Theory* **2002**, *37*, 1165–1177. [CrossRef]
26. Cabrera, J.A.; Ortiz, A.; Nadal, F.; Castillo, J.J. An evolutionary algorithm for path synthesis of mechanisms. *Mech. Mach. Theory* **2011**, *46*, 127–141. [CrossRef]
27. Rao, A.C. A Genetic Algorithm for Topological Characteristics of Kinematic Chains. *J. Mech. Des.* **2000**, *122*, 228–231. [CrossRef]

28. Liu, Y.; McPhee, J. Automated Kinematic Synthesis of Planar Mechanisms with Revolute Joints. *Mech. Based Des. Struct. Mach.* **2007**, *35*, 405–445. [CrossRef]
29. Lin, W.Y. A GA–DE hybrid evolutionary algorithm for path synthesis of four-bar linkage. *Mech. Mach. Theory* **2010**, *45*, 1096–1107. [CrossRef]
30. Baigunchekov, Z.; Laribi, M.A.; Carbone, G.; Dong, Z.; Kaiyrov, R. Structural-Parametric Synthesis of Path Generating Mechanisms. In *Advances in Mechanism and Machine Science*; Springer: Cham, Switzerland, 2023; Volume 147, pp. 300–309. [CrossRef]
31. Sarkisyan, Y.L.; Gupta, K.C.; Roth, B. Kinematic Geometry Associated With the Least-Square Approximation of a Given Motion. *J. Eng. Ind.* **1973**, *95*, 503–510. [CrossRef]
32. Starns, G.; Flugrad, D.R. Five-Bar Path Generation Synthesis by Continuation Methods. *J. Mech. Des.* **1993**, *115*, 988–994. [CrossRef]
33. Subbian, T.; Flugrad, D.R. Six and Seven Position Triad Synthesis Using Continuation Methods. *J. Mech. Des.* **1994**, *116*, 660–665. [CrossRef]
34. Galán-Marín, G.; Alonso, F.J.; Del Castillo, J.M. Shape optimization for path synthesis of crank-rocker mechanisms using a wavelet-based neural network. *Mech. Mach. Theory* **2009**, *44*, 1132–1143. [CrossRef]
35. Deshpande, S.; Purwar, A. Computational creativity via assisted variational synthesis of mechanisms using deep generative models. *J. Mech. Des. Trans.* **2019**, *141*, 121402. [CrossRef]
36. Sohoni, V.; Haug, E.J. A State Space Method for Kinematic Optimization of Mechanisms and Machines. *J. Mech. Des.* **1982**, *104*, 101–107. [CrossRef]
37. Ogot, M.M.; Gilmore, B.J. An Automated Procedure for the Maximization of the Mechanical Advantage of Planar Mechanisms. In Proceedings of the International Design Engineering Technical Conferences and Computers and Information in Engineering Conference, Santa Clara, CA, USA, 18–22 August 1991; Volume 2, pp. 311–319. [CrossRef]
38. Krishnamurty, S.; Turcic, D.A. Optimal synthesis of mechanisms using nonlinear goal programming techniques. *Mech. Mach. Theory* **1992**, *27*, 599–612. [CrossRef]
39. Kim, W.R.; Jung, J.H.; Ha, J.U.; Lee, D.H.; Shim, J.K. Data-Driven Dimensional Synthesis of Diverse Planar Four-Bar Function Generation Mechanisms via Direct Parameterization. Available online: https://arxiv.org/pdf/2507.08269 (accessed on 30 July 2025).
40. Zhang, Y.; Deng, X.; Zhou, B.; Zhao, P. Design and Optimization of a Multi-mode Single-DOF Watt-I Six-Bar Mechanism with One Adjustable Parameter. In *Advances in Mechanism, Machine Science and Engineering in China*; Springer: Singapore, 2023; pp. 1373–1390. [CrossRef]
41. Lu, X.; Lin, C.S. A Proposed Method to Group the Solutions From Dimensional Synthesis: Planar Triads for Six Precision Position. In Proceedings of the International Design Engineering Technical Conferences and Computers and Information in Engineering Conference, Scottsdale, AZ, USA, 13–16 September 1992; Volume Part F168016-3, pp. 481–487. [CrossRef]
42. Myszka, D.H.; Murray, A.P. Identifying sets of four and five positions that generate distinctive center-point curves. In Proceedings of the International Design Engineering Technical Conferences and Computers and Information in Engineering Conference, San Diego, CA, USA, 30 August–2 September 2009; Volume 7, pp. 463–473. [CrossRef]
43. McCarthy, J.M. Opposite pole quadrilateral as a compatibility linkage for parameterizing the center point curve. *J. Mech. Des. Trans.* **1993**, *115*, 332–336. [CrossRef]
44. Sandor, G.N.; Wilt, D.R. Optimal synthesis of a geared four-link mechanism. *J. Mech.* **1969**, *4*, 291–302. [CrossRef]
45. Rao, A.V.M.; Sandor, G. Extension of Freudenstein's Equation to Geared Linkages. *J. Eng. Ind.* **1971**, *93*, 201–210. [CrossRef]
46. Loerch, R.J.; Erdman, A.G.; Sandor, G.N. On the Existence of Circle-Point and Center-Point Circles for Three-Precision-Point-Dyad Synthesis. *J. Mech. Des.* **1979**, *101*, 554–562. [CrossRef]
47. Mather, S.; Erdman, A.G. Expansion of MK Circle Theory for Dyads and Triads. *Machines* **2023**, *11*, 841. [CrossRef]
48. Mlinar, J.R.; Erdman, A.G. An Introduction to Burmester Field Theory. *J. Mech. Des.* **2000**, *122*, 25–30. [CrossRef]
49. Mirth, J.A. Quasi-precision position synthesis of four-bar linkages. In Proceedings of the International Design Engineering Technical Conferences and Computers and Information in Engineering Conference, Minneapolis, MN, USA, 11–14 September 1994; Volume Part F167892-2, pp. 215–220. [CrossRef]
50. Mirth, J.A. The synthesis of planar linkages to satisfy an approximate motion specification. In Proceedings of the International Design Engineering Technical Conferences and Computers and Information in Engineering Conference, Albuquerque, NM, USA, 19–22 September 1993; Volume Part F167972-2, pp. 65–71. [CrossRef]
51. Faik, S.; Erdman, A.G. Sensitivity Distribution in the Synthesis Solution Space of Four-Bar Linkages. *J. Mech. Des.* **1991**, *113*, 3–9. [CrossRef]
52. Sharfi, O.M.A.; Smith, M.R. A simple method for the allocation of appropriate tolerances and clearances in linkage mechanisms. *Mech. Mach. Theory* **1983**, *18*, 123–129. [CrossRef]
53. Baumgarten, J.R.; Van Der Werff, K. A probabilistic study relating to tolerancing and path generation error. *Mech. Mach. Theory* **1985**, *20*, 71–76. [CrossRef]

54. Coit, W.G.; Riley, D.R. Sensitivity analysis of the inverted slider crank straight-line generator. *Mech. Mach. Theory* **1981**, *16*, 303–310. [CrossRef]
55. Lee, M.Y.; Erdman, A.G.; Faik, S. A Generalized Performance Sensitivity Synthesis Methodology for Four-Bar Mechanisms. In Proceedings of the International Design Engineering Technical Conferences and Computers and Information in Engineering Conference, Scottsdale, AZ, USA, 13–16 September 1992; Volume Part F1680, pp. 1–4. [CrossRef]
56. Soriano-Heras, E.; Pérez-Carrera, C.; Rubio, H. Mathematical Dimensional Synthesis of Four-Bar Linkages Based on Cognate Mechanisms. *Mathematics* **2024**, *13*, 11. [CrossRef]

Disclaimer/Publisher's Note: The statements, opinions and data contained in all publications are solely those of the individual author(s) and contributor(s) and not of MDPI and/or the editor(s). MDPI and/or the editor(s) disclaim responsibility for any injury to people or property resulting from any ideas, methods, instructions or products referred to in the content.